Research Article | Vol. 30, No. 25 / 5 Dec 2022 / Optics Express 45393
Optics EXPRESS

FBG array based wavelength calibration scheme for Fourier domain mode-locked laser with pm resolution and hourly stability

XIAOYU YANG,[1] MUXIN JIA,[1] GUI XIAO,[1] QUAN CHAI,[1] RENLAI ZHOU,[1] ROMAN V. ROMASHKO,[2] AND JIANZHONG ZHANG[1,*]

[1]*Key Lab of In-Fiber Integrated Optics, Ministry Education of China, Harbin Engineering University, Harbin 150001, China*
[2]*Institute for Automation and Control Processes of FEB RAS, 5 Radio St., Vladivostok, 690041, Russia*
[*]*zhangjianzhong@hrbeu.edu.cn*

Abstract: We demonstrate a fiber Bragg grating (FBG) array based wavelength calibration scheme for Fourier domain mode-locked (FDML) laser. The wavelength interval and the temperature feedback module of the FBG array are designed to ensure the reference stability of the wavelength calibration scheme. Combined with the calibration scheme, the FDML laser with a tunable wavelength range of ~60 nm, a center wavelength of 1300 nm and a sweep frequency of 39.63 kHz is built up to demonstrate its feasibility. The FBG wavelength demodulation based on the calibrated FDML laser system shows a wavelength resolution of 2.76 pm and hourly stability of 10.22 pm.

1. Introduction

The concept of the swept laser was first proposed in 1997 [1]. It has developed into a wide variety, including the use of grating rotating polyhedral mirror [2], grating galvanometer [3], fiber Fabry-Perot tunable filter (FFP-TF) [4] as filter devices and the dispersion tunable swept laser [5]. But the sweep speed of short cavity swept lasers is limited by repeating the process of spontaneous emission.

In 2006, R. Huber et.al proposed the concept of Fourier domain mode-locked (FDML) lasers based on a kilometer-length delay fiber and traditional tunable filter [6]. Using FDML technology, the maximum scanning rate limit caused by the photon lifetime of the laser cavity can be overcome by driving the optical filter synchronously with the optical round-trip time of the intracavity light wave. FDML laser has the advantages of MHz sweep speed [7], and a large tuning range of hundreds of nanometers [8]. FDML laser is widely used in optical coherence tomography (OCT) systems and has made remarkable achievements in retinal imaging, angiography and embryo imaging [9–11]. The FDML laser also provides a new method to measure spectrum in the time domain, as an important part of the spectrometer [12]. It plays an important role in optical fiber sensing [13] and spectroscopy [14–16].

Currently, the FDML laser has nonlinear problems. This nonlinear problem, temperature fluctuations and drive voltage fluctuations of the filter jointly cause the laser wavelength drift [7,17]. Here we refer to them collectively as the nonlinear problem. The nonlinear problem can be solved by particle swarm optimization algorithm and neural network modeling in low-frequency operation [18,19]. It becomes difficult in high-frequency operation (tens of kHz), which is the case with most proposed FDML lasers. Some scientists have proposed solutions to the nonlinear problem in FDML laser, including using gas cell or interferometer to calibrate the wavelength [20]. The wavelength band of the gas cell calibration method is strictly limited.

#475043 https://doi.org/10.1364/OE.475043
Journal © 2022 Received 7 Sep 2022; revised 30 Oct 2022; accepted 9 Nov 2022; published 30 Nov 2022

Optics EXPRESS

Interferometer calibration methods include the comb filter, the Fabry-Perot etalon, the Mach-Zehnder Interferometer (MZI) and the Sagnac interference loop [21–23]. These methods are affected by polarization, which causes peak finding difficult, reducing system accuracy and stability. In 2021, a high-speed spectrometer with FDML laser, Mach-Zehnder Interferometer (MZI), single peak filter and comb filter is proposed as the FBG interrogation tool [15], which achieved stability of 100 pm in 54 nm at 59.59 kHz and an average wavelength resolution of 21.85 pm. This wavelength calibration scheme is the highest resolution and stability achieved so far, but there is still a lot of room for improvement by reducing the polarization effect

Here, we propose a FBG array based wavelength calibration scheme for FDML laser. It has the characteristics of high accuracy, high stability, simple structure and easy packaging. The FBG reduces the effects of polarization. We have comprehensively considered the environment temperature, the delay of each optical path, the spatial position of different FBGs, and the FBG interrogation method. Combined with the FBG array, the FDML laser achieved a scanning frequency of 39.63 kHz within 60 nm around the central wavelength of 1300 nm. We achieved a wavelength calibration resolution of 2.76 pm and the stability of continuous operation for one hour is 10.22 pm.

2. Principle and experiment

The traditional swept laser can be produced only by transmitting the longitudinal mode of frequency through the narrow-band filter. When the center frequency of the narrow-band filter is tuned in the frequency sweeping process, each new frequency position of the filter must generate laser radiation by spontaneous emission. The maximum frequency tuning rate that can be achieved is limited by the characteristic time constant of enhancing laser activity in the cavity, and the FDML laser overcomes this limitation by adding a delay fiber to the traditional swept laser. When the transmission window of the optical bandpass filter is adjusted to the same optical frequency, the light from the primary frequency scanning propagates through the cavity and returns to the filter. In this structure, all wavelength modes can form resonances in the cavity at the same time, so as to obtain a quasi-continuous output. Therefore, the sweep speed only depends on the tuning speed of the filter.

The Schematic diagram of the FDML laser is shown in Fig. 1 in the central area. The FDML laser is a ring cavity structure composed of a semiconductor optical amplifier (SOA, InPhenix, Inc.) with a gain maximum centered at 1300 nm as a gain medium, and a FFP-TF (Lambda Quest) with a fineness of 977.5 and a free spectral range of 137 nm at 1300 nm as the sweep filter. The temperature coefficient of the FFP-TF used is lower than 1 nm/°C. The limit drive frequency of FFP-TF is 40 kHz. Two optical isolators (ISO) ensure unidirectional lasing. A single-mode optical fiber (YOFC, FullBand) is used as delay optical fiber with a total length L = 10.2 km and an effective refractive index n_{eff} = 1.466, loss of 0.33 dB/km. The fundamental frequency is obtained at the scanning frequency of FFP-TF f_{drive} = 19.815 kHz. The stable drive signal of the FFP-TF is provided by the signal generator (RIGOL, DG1062Z). Because the filter is a capacitive load with a low impedance of 0.4 μF. Using the signal generator alone will cause distortion and a narrow voltage range. Therefore, a power amplifier module (PA, OPA549) is added at the back end of the signal generator. At the output optical coupler (OC), 20% of the optical signal is converted into the electrical signal by a photodetector (PD, Thorlabs, PDB450c) and displayed by an oscilloscope (OSC, Tektronix, MSO64) to characterize the scanning signal and 80% of the output signal is returned to the ring cavity. The experiments were conducted on a shockproof platform with heat dissipation and temperature control. The tunable wavelength range of the FDML laser, shown in Fig. 2. (a), can be detected by an optical spectrum analyzer (OSA, Ando, AQ6317C). The obvious distortion comes from the scanning speed difference of the FFP-TF dived by a sine function voltage and the mismatch between the tunable speed of the FDML laser and the scanning speed of OSA. The output laser intensity can't be well demonstrated because of

Optics EXPRESS

the fast tuning speed of the laser wavelength, which can be detected by PD and shown in Fig. 2. (b). The transient intensity curve of the FDML laser, including forward sweep (short to long wavelength) and backward sweep (long to short wavelength). The FDML laser with a sweep speed of 39.63 kHz, a center wavelength of about 1300 nm, and a range greater than 60 nm can be obtained.

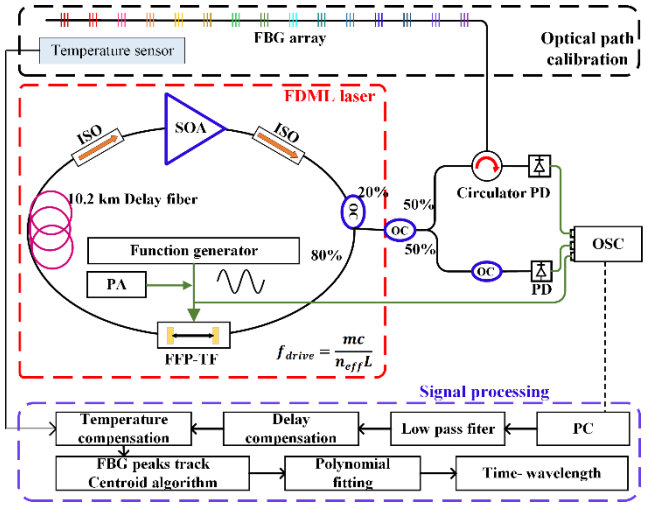

Fig. 1. Schematic diagram of the Fourier domain mode-locked (FDML) laser.

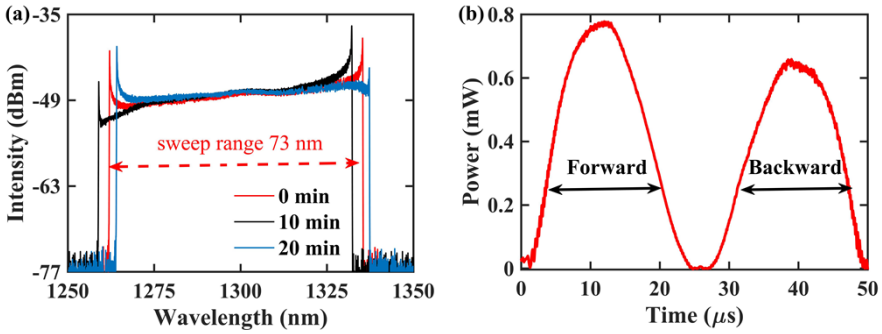

Fig. 2. (a) Optical spectrum of the FDML laser output measured at different moments of operation time, (b) The FDML laser output power temporal evolution during one scamming cycle.

Since the FFP-TF in the FDML laser is a capacitive load, there are the following problems when measuring spectrum directly with the FDML laser: (1) FFP-TF is nonlinear, including hysteresis and creep; Hysteresis is most severe at the start and end voltages. (2) FFP-TF is affected by temperature and other environmental factors. The above problems lead to the uncertainty of the output laser wavelength of the FDML laser. It can be seen from Fig. 2. (a) that the spectrum of the FDML laser continues to drift with the increase of operation time, and the moving range is within 5 nm, which is caused by the nonlinearity of the filter. Due to the nonlinearity of the voltage-to-wavelength relationship, converting voltage to wavelength in linear relationships is inaccurate. Here, we propose the FBG array as a wavelength calibration method. The FBG array is composed of 15 FBGs connected in series from short wavelength to long wavelength. The

Optics EXPRESS

wavelength of the FBG array measured by OSA is used to calibrate the wavelength of the FDML laser. The parameters of the FBG array are shown in Table 1. As shown in Fig. 1, the laser output and the FBG array reflection signal (see the optical path calibration area) are detected in parallel. These two signals keep synchronous output in time to realize wavelength calibration. Since a sine signal is used to drive FFP-TF, the nonlinearity at both ends of the spectral range covering the FBG array wavelengths is more serious than that in its middle. To improve the utilization of the FBG array, the arrangement method of dense at both ends and sparse in the middle is adopted.

Table 1. Parameters of the 15 FBGs

Wavelength (nm)	1269.56	1273.03	1276.08	1280.30	1285.14	1290.10	1295.28	1300.20	1305.44	1309.80	1315.22	1320.16	1323.21	1327.02	1330.16
Reflectivity (%)	98.9	95.0	97.9	94.6	95.9	96.8	95.2	95.2	92.5	99.8	97.9	94.1	96.8	92.3	98.5
Loss (dB)	0.09	0.12	0.36	0.26	0.31	0.44	0.31	0.31	0.26	0.30	0.31	0.31	0.31	0.35	0.40

Nonlinearity is more severe at the peaks and valleys of the drive signal. The FBG array of different wavelength densities is used to ensure overall accuracy. The FBG spacing in the middle (40 nm) part of the spectral range is 5 nm. Four FBGs are located in the 10 nm range at each end of the FBG array. There are Fifteen FBGs in the range of 1270-1330 nm. Then the FBG array is sealed to avoid the disturbance of environmental factors such as vibration. To avoid the influence of temperature, a temperature sensor module with an accuracy of 0.1 ℃ is added as temperature compensation.

The results of the FBG array calibration optical path in the time domain are shown in Fig. 3. Both the laser output and the calibration channels are collected on the OSC through the 100 MHz bandwidth PD respectively. The power distribution in Fig. 3. (b) is caused by the FDML laser power distribution in the ring cavity, the reflectivity and the loss of 15 FBGs. The short wavelength (25μs) travel a shorter distance than the long wavelength (0μs) and is less affected by the loss. The detailed reflectivity and loss of 15 FBGs are listed in Table1. As shown in the signal processing part of Fig. 1. To ensure the time synchronization of each signal, accurate time compensation is necessary. Time compensation includes the delay between each optical path and the delay of each FBG. The time of calibrating the optical path reflects the change in laser wavelength and the wavelength value of the laser can be calculated. Here, we use band-pass filtering to remove the system noise effect. Using the centroid algorithm, the reflected light power is used as the weighting coefficient, and the weighted average value is calculated, which directly reflects the power distribution, so as to obtain the time point corresponding to the central wavelength. The time-wavelength relationship is obtained by polynomial (with third degree) fitting. Finally, obtained the time-wavelength curve in the range of 60 nm is shown in Fig. 4. (a). Of course, At 39.63 kHz sweep frequency, the wavelength dependency can fall behind from the drive voltage. This causes the FFP-TF voltage-to-wavelength hysteresis loop shown in Fig. 4. (b) which is to be taken into account during the design of the FDML laser.

FDML lasers based on the wavelength calibration scheme can be used for spectrum measurement. To test wavelength calibration accuracy and stability, we selected 11 FBGs at different positions in the range of 60 nm. Both the central wavelength and spectral shape of these FBGs are measured. Characterization of average wavelength resolution and system stability with standard deviation and fluctuation range of 11 FBGs. The driving signal which provided the operation of the system was kept unchanged for 60 minutes. Three FBGs from the 11 FBGs located in the beginning, in the middle and at the end of the spectral range 1270-1330 nm: FBG1 (1274.8 nm), FBG2 (1309.7 nm), and FBG3 (1324.9 nm). Figure 5. (a, b, c) shows the temporal evolution of the central wavelength for three of these FBGs. As seen the standard deviation of the central wavelength for FBG2 which is located in the middle band is 2.14 pm. FBG1 and FBG3 located at both ends reveal the larger standard deviation, 2.62 pm and 3.46 pm, respectively. Since the number of FBGs at both ends is denser, the standard deviation of the three FBGs is not much

Optics EXPRESS

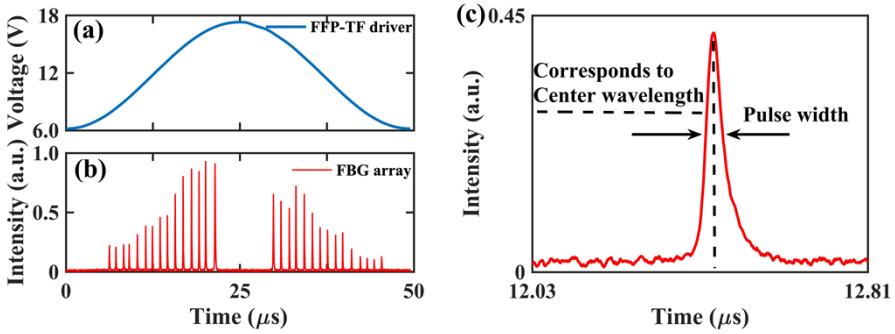

Fig. 3. Output from FFP-TF driver (a) the FBG array (b) and single FBG (c).

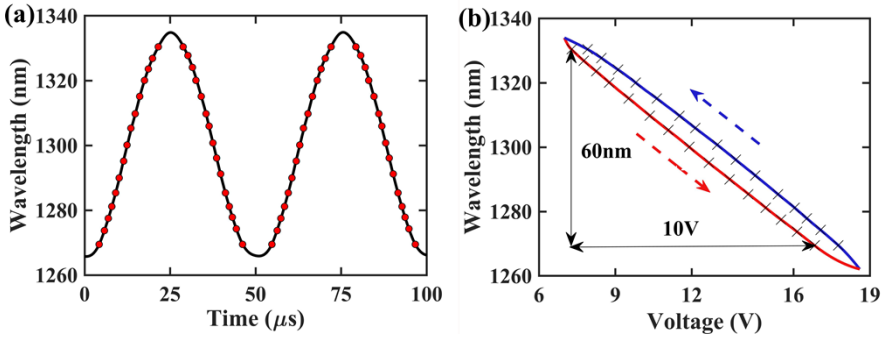

Fig. 4. (a) Time-wavelength curve obtained by fitting, (b) FFP-TF voltage-to-wavelength hysteresis loop.

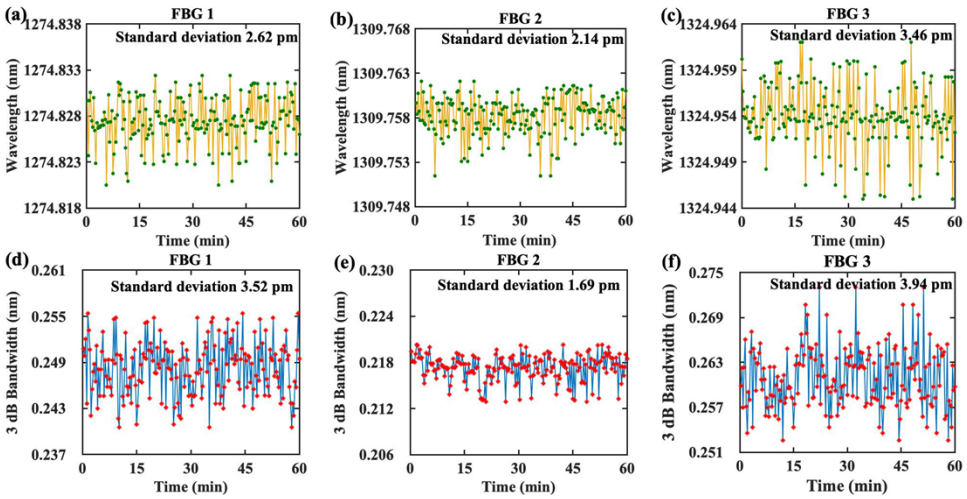

Fig. 5. Wavelength resolution and system stability test: temporal evolution of central wavelength (a, b, c) is the yellow curve and 3 dB bandwidth for three FBGs (d, e, f) is the blue curve.

Optics EXPRESS

different. The fluctuation range of the central wavelength of the three FBG is 1274.82 ± 0.006 nm, 1309.75 ± 0.005 nm and 1324.95 ± 0.009 nm. Figure 5. (d, e, f) shows the fluctuation of the 3 dB bandwidth of three FBGs. The 3 dB bandwidth is the pulse width shown in Fig. 3. (c) converted from the time-wavelength curve. The bandwidth of FBG2 is 0.21 ± 0.004 nm, and the standard deviation for one-hour running is 1.69 pm. Figure 6 summarizes the standard deviation of central wavelength and 3 dB bandwidth of 11 FBGs with different wavelengths within 60 minutes. The central wavelength and 3 dB bandwidth of 11 FBGs have a maximum fluctuation range of ±10.22 pm under continuous operation for one hour. The results between OSA and the FDML laser based system are well matched. In the system, the FBG array structure we designed successfully solved the nonlinearity problem, enabling accurate measurement of wavelengths in the time domain. The system continuous operation for one hour has obtained an average wavelength resolution of 2.76 pm and stability of 10.22 pm, which has been confirmed.

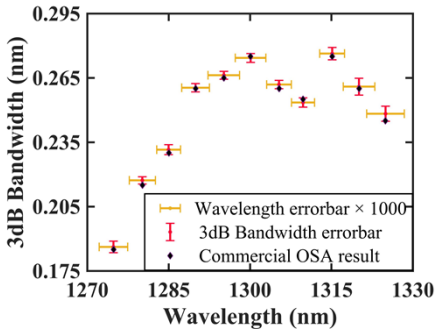

Fig. 6. Spectral resolution of all 11 FBGs during 60 minutes of the system operation, and commercial OSA test results.

3. Conclusion

In conclusion, we propose a calibration method that ensures accurate detection of the wavelength of the FDML laser system. The system has the capability of high speed and high precision spectrum measurement, which is very useful for FBG sensor demodulation. Within the scanning frequency of 39.63 kHz and the whole spectral range of 60 nm, the average wavelength calibration resolution of 2.76 pm and stability of 10.22 pm have been achieved at continuous operation for one hour.

Funding. National Natural Science Foundation of China (61775045, 62005063, 62005064); National Key Research and Development Program of China (2021YFC2802202); Science Fund for Distinguished Young Scholars of Heilongjiang Province (JQ2022F001).

Disclosures. The authors declare that there are no conflicts of interest related to this article.

Data availability. Data underlying the results presented in this paper are not publicly available at this time but may be obtained from the authors upon reasonable request.

References

1. S. R. Chinn, E. A. Swanson, and J. G. Fujimoto, "Optical coherence tomography using a frequency-tunable optical source," Opt. Lett. **22**(5), 340–342 (1997).
2. W. Y. Oh, S. H. Yun, G. J. Tearney, and B. E. Boumar, "115 kHz tuning repetition rate ultrahigh-speed wavelength-swept semiconductor laser," Opt. Lett. **30**(23), 3159–3161 (2005).
3. V. J. Srinivasan, R. Huber, I. Gorczynska, J. G. Fujimoto, J. Y. Jiang, P. Reisen, and A. E. Cable, "High-speed, high-resolution optical coherence tomography retinal imaging with a frequency-swept laser at 850 nm," Opt. Lett. **32**(4), 361–363 (2007).
4. R. Huber, M. Wojtkowski, K. Taira, J. G. Fujimoto, and K. Hsu, "Amplified, frequency swept lasers for frequency domain reflectometry and OCT imaging: design and scaling principles," Opt. Express **13**(9), 3513–3528 (2005).

Optics EXPRESS

5. J. Kang, P. Feng, X. Wei, E. Y. Lam, K. K. Tsia, and K. K. Y. Wong, "102-nm, 44.5-MHz inertial-free swept source by mode-locked fiber laser and time stretch technique for optical coherence tomography," Opt. Express **26**(4), 4370–4381 (2018).
6. R. Huber, M. Wojtkowski, and J. G. Fujimoto, "Fourier Domain Mode Locking (FDML): A new laser operating regime and applications for optical coherence tomography," Opt. Express **14**(8), 3225–3237 (2006).
7. T. Pfeiffer, M. Petermann, W. Draxinger, C. Jirauschek, and R. Huber, "Ultra low noise Fourier domain mode locked laser for high quality megahertz optical coherence tomography," Biomed. Opt. Express **9**(9), 4130–4148 (2018).
8. S. H. Kassani, M. Villiger, N. Uribe-Patarroyo, C. Jun, R. Khazaeinezhad, N. Lippok, and B. E. Bouma, "Extended bandwidth wavelength swept laser source for high resolution optical frequency domain imaging," Opt. Express **25**(7), 8255–8266 (2017).
9. R. A. Leitgeb, "En face optical coherence tomography: a technology review [Invited]," Biomed. Opt. Express **10**(5), 2177–2201 (2019).
10. A. Zhang, Q. Zhang, C.-L. Chen, and R. K. Wang, "Methods and algorithms for optical coherence tomography-based angiography: a review and comparison," J. Biomed. Opt. **20**(10), 100901 (2015).
11. R. Raghunathan, M. Singh, M. E. Dickinson, and K. V. Larin, "Optical coherence tomography for embryonic imaging: a review," J. Biomed. Opt. **21**(05), 1 (2016).
12. D. Huang, Y. Shi, F. Li, and P. K. A. Wai, "Fourier Domain Mode Locked Laser and Its Applications," Sensors **22**(9), 3145 (2022).
13. E. J. Jung, C. S. Kim, M. Y. Jeong, M. K. Kim, M. Y. Jeon, W. Jung, and Z. Chen, "Characterization of FBG sensor interrogation based on a FDML wavelength swept laser," Opt. Express **16**(21), 16552–16560 (2008).
14. T. Yamaguchi, W. Endo, and Y. Shinoda, "Real-Time Spectroscopy System for Continuous Measurement With Fourier-Domain Mode-Locked Laser at 1550 nm," IEEE Sens. Lett. **5**(8), 1–4 (2021).
15. X. Zhang, Y. Hu, Y. Yang, and Y. Wang, "Research On High Speed Spectrum Analyzer Based On Fourier Domain Mode Locked Laser," in *6th International Conference on Smart Grid and Electrical Automation* (ICSGEA, 2021), pp. 597–600.
16. L. A. Kranendonk, X. An, A. W. Caswell, R. E. Herold, S. T. Sanders, R. Huber, J. G. Fujimoto, Y. Okura, and Y. Urata, "High speed engine gas thermometry by Fourier-domain mode-locked laser absorption spectroscopy," Opt. Express **15**(23), 15115–15128 (2007).
17. K. Liu, W. C. Jing, G. D. Peng, J. Z. Zhang, D. G. Jia, H. X. Zhang, and Y. M. Zhang, "Investigation of PZT driven tunable optical filter nonlinearity using FBG optical fiber sensing system," Opt. Commun. **281**(12), 3286–3290 (2008).
18. H. Ding, X. Wu, J. Liang, and X. Li, "Online calibration of PZT driven fiber Fabry–Perot filter nonlinearity using FBG array and PSO algorithm," Measurement **42**(7), 1059–1064 (2009).
19. L. Zhang, Z. Zhu, X. Zhou, and L. Sun, "Model Reference Adaptive Control of Cross-Coupling Hysteresis in Piezoceramics With Dynamic Loads," IEEE Access **10**, 14691–14697 (2022).
20. X. Fan, J. Jiang, X. Zhang, K. Liu, S. Wang, Y. Yang, F. Sun, J. Zhang, C. Guo, J. Shen, S. Wu, and T. Liu, "Self-marked HCN gas based FBG demodulation in thermal cycling process for aerospace environment," Opt. Express **26**(18), 22944–22953 (2018).
21. J. Mei, X. Xiao, and C. Yang, "Delay compensated FBG demodulation system based on Fourier domain mode-locked lasers," IEEE Photonics Technol. Lett. **27**(15), 1585–1588 (2015).
22. Q. Liu, Y. Wang, Z. Li, Y. Hou, Z. Xu, and X. Gui, "An Integrated Design of Ultra-High-Speed FBG Interrogation System-Based on FDML Laser," IEEE Photonics Technol. Lett. **32**(19), 1245–1248 (2020).
23. H. D. Lee, E. J. Jung, M. Y. Jeong, and C. S. Kim, "Linearized interrogation of FDML FBG sensor system using PMF Sagnac interferometer," in *20th International Conference on Optical Fibre Sensors* (SPIE, 2009), pp. 743–746.